Frustrated spin ladder with alternating spin-1 and spin-$\frac{1}{2}$ rungs

V. Ravi Chandra,[1,2] N. B. Ivanov,[3,4] and J. Richter[5]

[1]*Max-Planck-Institute for Physics of Complex Systems, Nöthnitzer Str. 38, D-01187 Dresden, Germany*
[2]*Physics Department, The Technion, Haifa 32000, Israel*
[3]*Fakultät für Physik, Universität Bielefeld, D-33501 Bielefeld, Germany*
[4]*Institute of Solid State Physics, Bulgarian Academy of Sciences, Tzarigradsko Chaussee 72, 1784 Sofia, Bulgaria*
[5]*Institut für Theoretische Physik, Universität Magdeburg, PF 4120, D-39016 Magdeburg, Germany*

We study the impact of the diagonal frustrating couplings on the quantum phase diagram of a two-leg ladder composed of alternating spin-1 and spin-$\frac{1}{2}$ rungs. As the coupling strength is increased the system successively exhibits two gapped paramagnetic phases (a rung-singlet and a Haldane-type nondegenerate states) and two ferrimagnetic phases with different ferromagnetic moments per rung. The first two states are similar to the phases studied in the frustrated spin-$\frac{1}{2}$ ladder, whereas the magnetic phases appear as a result of the mixed-spin structure of the model. A detailed characterization of these phases is presented using density-matrix renormalization-group calculations, exact diagonalizations of periodic clusters, and an effective Hamiltonian approach inspired by the analysis of numerical data. The present theoretical study was motivated by the recent synthesis of the quasi-one-dimensional ferrimagnetic material $Fe^{II}Fe^{III}$ (trans-1,4-cyclohexanedicarboxylate) exhibiting a similar ladder structure.

PACS number(s): 75.10.Jm, 75.50.Gg, 64.70.Tg

I. INTRODUCTION

Over the past two decades there has been an increasing interest in quantum spin systems with competing exchange interactions.[1,2] Quantum spin chains and ladders with frustration, both for half integer and integer spins, set up an important part of this research since they provide a unique testing ground based on the available powerful analytical and numerical techniques for one-dimensional (1D) systems. In particular, the frustrated ladder models have allowed controlled calculations to examine topological order,[3] dimer order,[4] as well as the appearance of fractional excitations in spin models.[5] Most of previously studied frustrated chain and ladder models have been related to uniform-spin structures with all the spins same. In comparison, till now much less experimental as well as theoretical work concerning the impact of competing interactions in quasi-1D mixed-spin systems has been accomplished.[6] Often these systems exhibit quasi-1D ferrimagnetic ground states with a net ferromagnetic moment so that apart from rich quantum phase diagrams they might be expected to provide generic examples of 1D magnetic-paramagnetic quantum phase transitions.[7]

On the experimental side, during the past two decades it has become possible to synthesize a large variety of quasi-1D materials with ferrimagnetic properties. Most of these materials are heterometallic molecular magnets containing different transition metal ions in the unit cell.[8] A generic spin model describing these materials is the quantum Heisenberg spin chain with antiferromagnetic nearest-neighbor exchange interactions and two types of alternating quantum spins with magnitudes S_1 and $S_2(S_1 > S_2)$.[9–11] In the extreme quantum case of spins (1,1/2), the latter model was shown to provide an excellent description of the thermodynamic parameters of the recently synthesized quasi-1D bimetallic compound $NiCu(pba)(D_2O)_3 \cdot 2D_2O(pba = 1,3$-propylenebis).[12] Another important class of quasi-1D

ferrimagnets—the so-called topological ferrimagnets—is related to some homometallic materials exhibiting composite chain structures with different magnetic sublattices.[13] The homometallic material $A_3Cu_3(PO_4)_4(A = Ca, Sr, Pb)$ is an example of such quasi-1D ferrimagnets: in this compound, the Cu^{2+} ions form diamond chains with strongly coupled trimers bridged by oxygen ions.[14] Since quasi-1D homometallic materials usually have rich exchange pathway structures, they may be expected to provide some real examples of quasi-1D ferrimagnets with magnetic frustration. To the best of our knowledge, the recently synthesized mixed-valent magnetic material $Fe^{II}Fe^{III}$ (trans-1,4-cyclohexanedicarboxylate) (Ref. 15) provides the first real example of a quasi-1D Heisenberg ferrimagnet with magnetic frustration. The experimentally established magnetic structure for temperatures larger than 36 K corresponds to the mixed-spin ladder with diagonal exchange bonds shown in Fig. 1, where the site spins $S_1 = 5/2$ and $S_2 = 2$ are, respectively, related to the magnetic ions Fe^{III} and Fe^{II}.[15]

The mentioned experimental achievements motivated a series of theoretical studies on quantum mixed-spin chains
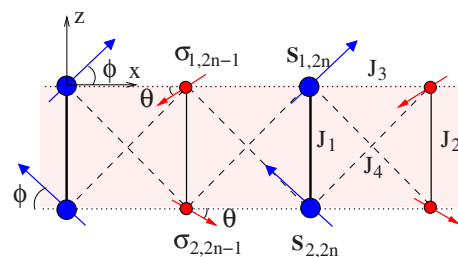
FIG. 1. (Color online) The mixed-spin ladder considered in the paper. The arrows show the classical canted state described by the angles $0 < \phi < \pi/2$ and $0 < \theta < \pi/2$ for the classical spins with magnitudes S_1 and S_2, respectively. The other two classical phases correspond to spin configurations with $(\phi, \theta) = (0,0)$ (antiferromagnetic state) and $(\phi, \theta) = (\pi/2, \pi/2)$ (ferrimagnetic state).

and ladders with geometric frustration. The symmetric diamond chain with antiferromagnetic vertical bonds was probably the first studied model of a 1D quantum ferrimagnet with competing interactions.[16] A variant of this model, the distorted spin-$\frac{1}{2}$ diamond chain, has received special theoretical[17] as well as experimental[18] interest due to its rich quantum phase diagram[19] and the relevance for the real material $Cu_3(CO_3)_2(OH)_2$. The diamond Heisenberg chain is also one of the simplest quantum spin models admitting four-spin cyclic exchange interactions.[20] A generic quantum spin model of a frustrated 1D ferrimagnet is the mixed-spin Heisenberg chain composed of two types of alternating spins interacting via competing nearest-neighbor and next-nearest-neighbor antiferromagnetic exchange bonds.[21] This model may also be considered as a mixed-spin zigzag ladder and is a ferrimagnetic analog of the frustrated Heisenberg chain with ferromagnetic nearest-neighbor and antiferromagnetic next-nearest-neighbor exchange bonds. The spin-$\frac{1}{2}$ frustrated J_1-J_2 ferromagnetic chain has recently attracted much attention,[22] as it is supposed to describe a number of quasi-1D edge-sharing cuprates, such as $Rb_2Cu_2Mo_3O_{12}$,[23] Li_2ZrCuO_4,[24] and $LiCuVO_4$.[25] The latter material exhibits multiferroic properties[26] as well as an interesting specific phase transition in a magnetic field from an ordered spiral to an ordered modulated-collinear magnetic phases.[27] There are other two generic types of frustrated mixed-spin ladder models describing two interacting mixed-spin alternating chains. The first one is the checkerboard mixed-spin Heisenberg ladder with frustrating diagonal exchange couplings[28] and the second one is the two-leg ladder model with two types of alternating rungs presented in Fig. 1. Finally, there has been a lot of recent work reporting interesting quantum phase diagrams in different composite Heisenberg chains with ferrimagnetic ground states.[29]

In this study we focus on the effects of frustration on the ground-state phase diagram of the mixed-spin ladder shown in Fig. 1. In addition to the theoretically interesting question of the effects of frustration in this system, an experimental realization of a closely related system in a mixed-valence iron polymer further motivates us.[15] In the next section we introduce the model and study some relevant properties of its Hamiltonian. In Sec. III, we give a detailed description of the quantum phases by using an effective Hamiltonian approach inspired by the analysis of data obtained using density-matrix renormalization-group (DMRG) and exact-diagonalization (ED) techniques. We conclude in Sec. IV with a brief summary of the results.

II. MODEL

The system under consideration (see Fig. 1) consists of two equivalent mixed-spin Heisenberg chains (characterized by the nearest-neighbor exchange constant $J_3 > 0$) coupled via rung ($J_1, J_2 > 0$) as well as diagonal ($J_4 \geq 0$) exchange bonds. The Hamiltonian of the system reads as

$$\mathcal{H} = \mathcal{H}_{12} + \mathcal{H}_3 + \mathcal{H}_4, \qquad (1)$$

where

$$\mathcal{H}_{12} = \sum_{n=1}^{L/2} (J_1 s_{1,2n} \cdot s_{2,2n} + J_2 \sigma_{1,2n-1} \cdot \sigma_{2,2n-1}),$$

$$\mathcal{H}_3 = J_3 \sum_{n=1}^{L/2} \sum_{m=1}^{2} [s_{m,2n} \cdot (\sigma_{m,2n-1} + \sigma_{m,2n+1})],$$

$$\mathcal{H}_4 = J_4 \sum_{n=1}^{L/2} [s_{1,2n} \cdot (\sigma_{2,2n-1} + \sigma_{2,2n+1})$$
$$+ s_{2,2n} \cdot (\sigma_{1,2n-1} + \sigma_{1,2n+1})].$$

Here $s_{k,2n}$ and $\sigma_{k,2n-1}(k=1,2)$ are, respectively, spin-S_1 and spin-S_2 operators ($S_1 > S_2$), and L is the number of rungs.

It is instructive to present the Hamiltonian in the following form

$$\mathcal{H} = \mathcal{H}_{12} + \sum_{n=1}^{L/2} [J_s s_{2n} \cdot (\sigma_{2n-1} + \sigma_{2n+1})] + J_a V, \qquad (2)$$

where $J_{s,a} = (J_3 \pm J_4)/2$, and $s_{2n} = s_{1,2n} + s_{2,2n}$, and $\sigma_{2n+1} = \sigma_{1,2n+1} + \sigma_{2,2n+1}$ are rung spin operators. The operator V reads as

$$V = \sum_{n=1}^{L/2} = L_{2n} \cdot (l_{2n-1} + l_{2n+1}), \qquad (3)$$

where $L_{2n} = s_{1,2n} - s_{2,2n}$ and $l_{2n\pm1} = \sigma_{1,2n\pm1} - \sigma_{2,2n\pm1}$ are rung vector operators. The following analysis of the zero-temperature quantum phase diagram addresses the extreme quantum case of spins $S_1 = 1$ and $S_2 = 1/2$, and is mainly restricted to the parameter subspace defined by $J_1 = J_2 = J_3 > 0$ and $J_4 \geq 0$. To some extent, such a choice of the parameters is motivated by the experimentally established strengths of the exchange couplings in the ferrimagnetic ladder material $Fe^{II}Fe^{III}$ (trans-1,4-cyclohexanedicarboxylate).[15]

A. Symmetries of the model

The mixed-spin system inherits some important symmetries of the parent uniform-spin Heisenberg ladder with diagonal interactions.[30] First, if the parameters J_3 and J_4 in $\mathcal{H}$ are exchanged, one can recover the original Hamiltonian by exchanging either the spins on the S_1 rungs ($s_{1,2n} \leftrightarrow s_{2,2n}$), or the spins on the S_2 rungs ($\sigma_{1,2n-1} \leftrightarrow \sigma_{2,2n-1}$). This means that $\mathcal{H}(J_1, J_2, J_3, J_4) = \mathcal{H}(J_1, J_2, J_4, J_3)$. Therefore, the study of the model can be restricted in the region $J_4/J_3 \leq 1$ since the model with $J_4/J_3 > 1$ maps onto the one with $J_4/J_3 < 1$. Because of the same symmetry, Hamiltonian (2) does not contain mixed products of rung spins and rung vector operators.

The second property of $\mathcal{H}$ concerns the subspace $J_3 = J_4$ ($J_a = 0$) when the last term in Eq. (2) disappears. As in the uniform-spin case,[31] in this parameter subspace the Hamiltonian $\mathcal{H}$ commutes with the local operators s_{2n}^2 and $\sigma_{2n-1}^2(n=1,2,\ldots,L/2)$, which means that the rung spins s_{2n} and σ_{2n-1} [defined as $s_{2n}^2 = s_{2n}(s_{2n}+1)$ and $\sigma_{2n-1}^2 = \sigma_{2n-1}(\sigma_{2n-1}+1)$] are good local quantum numbers. Thus in every sector of the Hilbert space, defined by the sequence $[\sigma_1, s_2, \ldots, \sigma_{L-1}, s_L]$, the first two terms in Eq. (2) reduce to the constant

$$E_0 = -\frac{L}{2}[J_1 S_1(S_1+1) + J_2 S_2(S_2+1)] + \frac{1}{2}\sum_{n=1}^{L/2}[J_1 s_{2n}(s_{2n}+1)$$

$$+ J_2 \sigma_{2n-1}(\sigma_{2n-1}+1)].$$

Thus Eq. (2) takes the simple form of a Heisenberg spin chain

$$\mathcal{H}_0 = E_0 + \sum_{n=1}^{L/2} J_s \mathbf{s}_{2n} \cdot (\boldsymbol{\sigma}_{2n-1} + \boldsymbol{\sigma}_{2n+1}). \tag{4}$$

The above expression for E_0 implies that for strong enough rung interactions $(J_1/J_3, J_2/J_3 \gg 1)$ the singlet eigenstate of Eq. (4), defined as a product of local rung-singlet (RS) states, becomes an exact ground state of the model. This state belongs to the sector $[0,0,\ldots,0,0]$ and can be considered as a prototype of the rung-singlet phase of Eq. (2) discussed below. The following analysis of the quantum phase diagram of Eq. (2) implies that in the extreme quantum limit $(S_1,S_2) = (1,1/2)$ the sectors $[1,1,\ldots,1,1]$, $[1,2,\ldots,1,2]$, and $[1,1,1,2,\ldots,1,1,1,2]$ also play an important role: in the first sector, the model defined by Eq. (4) is equivalent to the spin-1 Haldane chain, whereas in the last two sectors Eq. (4) represents spin-alternating ferrimagnetic chains. The ground states related to these models appear in the quantum phase diagram of the discussed system.

B. Classical phase diagram

The classical phases of Eq. (1) can be described by the angles ϕ and θ (see Fig. 1) which determine the orientations of the classical spins in the xz plane. We consider the parameter subspace defined by $J_1 = J_2 = J_3 = 1$ and $J_4 \ge 0$. The expression for the ground-state energy per cell containing two rungs is seen to be

$$\frac{E_c}{S_1 S_2} = -\frac{S_1}{S_2}\cos(2\phi) - \frac{S_2}{S_1}\cos(2\theta) - 4\cos(\phi-\theta)$$

$$+ 4J_4\cos(\phi+\theta). \tag{5}$$

A minimization using the independent angle variables ϕ and θ gives the following equations,

$$\cos(\phi+\theta) = \frac{c_1}{\kappa}J_4 - c_2,$$

$$\cos(\phi-\theta) = c_2 J_4 - c_1 \kappa, \tag{6}$$

where $c_1 = \sigma - \sigma^{-1}$, $c_2 = \sigma + \sigma^{-1}$, and $\sigma = S_1/S_2 > 1$. The parameter $\kappa = \kappa(J_4)$ reads $\kappa = (4J_4^2/3 - 1/3)^{1/2}$.

The lower $(J_4^{(d)})$ and the upper $(J_4^{(u)})$ phase boundaries of the classical canted phase shown in Fig. 1 are related to the inequalities $|\cos(\phi+\theta)|$, $|\cos(\phi-\theta)| \le 1$ implying

$$J_4^{(d)} = \frac{c_2+1}{\sqrt{4(c_2+1)^2 - 3c_1^2}},$$

$$J_4^{(u)} = \frac{c_2-1}{\sqrt{4(c_2-1)^2 - 3c_1^2}}. \tag{7}$$
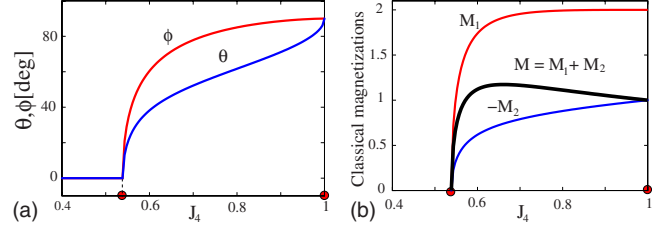
FIG. 2. (Color online) (a) The classical phase diagram described by the angles ϕ and θ vs J_4, as obtained from Eq. (6) for the system with $S_1 = 1$ and $S_2 = 1/2$. (b) z components of the classical magnetizations in the $S_1(M_1)$ and $S_2(M_2)$ sites of the same system. The filled circles on the J_4 axis correspond to the classical transition points $J_4^{(d)} = 7/13$ and $J_4^{(u)} = 1$.

For $J_4 < J_4^{(d)}$, we get states of zero magnetization in which the two spins on any rung and spins along a leg are antiferromagnetically aligned. The canted state realized for $J_4^{(d)} < J_4 < J_4^{(u)}$ has a net magnetization that takes a maximal value at some intermediate J_4 between both boundaries [see Fig. 2(b)]. For $J_4 > J_4^{(u)}$ this classical canted phase gives way to a ferrimagnetic state where all the spins of the same magnitude are ferromagnetically aligned but the relative alignment of S_1 and S_2 is antiferromagnetic. Notice that the magnetic measurements in Ref. 15 indicate the discussed ferrimagnetic configuration, eventually with a small canting of the classical spins, as the most probable spin configuration realized in the real material $Fe^{II}Fe^{III}$. For $S_1 = 1$ and $S_2 = 1/2$, the above equations give $J_4^{(d)} = 7/13 \approx 0.538$ and $J_4^{(u)} = 1$. For the real material studied in Ref. 15 $(S_1 = 5/2, S_2 = 2)$, one has $J_4^{(d)} = 61/121 \approx 0.504$ and $J_4^{(u)} = 21/39 \approx 0.553$.

Interestingly, the discussed classical ferrimagnetic state appears only for relatively small values of σ. For larger σ, the lowest-energy collinear configuration for large J_4 is a nonmagnetic state with ferromagnetically arranged legs pointing in opposite directions (i.e., antiferromagnetically aligned rungs). Comparing the energies of both configurations $(E_c^{(1)} = S_1^2 + S_2^2 - 4S_1 S_2 - 4S_1 S_2 J_4$, $E_c^{(2)} = -S_1^2 - S_2^2 + 4S_1 S_2 - 4S_1 S_2 J_4$, respectively), we see that the ferrimagnetic configuration is realized only in the interval $1 < \sigma \le 2 + \sqrt{3} \approx 3.73$. In the large σ case, the canted phase is also modified: on increasing the parameter J_4 from $J_4^{(d)}$ up to $J_4^{(u)}$, the S_2 spins smoothly change their orientation by π, whereas the net orientation of the larger S_1 spins coincides at the phase boundaries. In both variants of the classical phase diagram the phase boundaries are defined by Eq. (7).

Finally, the discussed classical phase diagrams were independently confirmed by our classical Monte Carlo simulations. Below we argue that the classical ferrimagnetic phase survives quantum fluctuations, whereas both the antiferromagnetic as well as the canted classical phases are completely destroyed.

III. QUANTUM PHASE DIAGRAM

We consider the parameter subspace defined by $J_1 = J_2 = J_3 = 1$ and $0 \le J_4 \le 1.5$, and use the DMRG method[32] for open boundary conditions supplemented by ED data for periodic clusters containing up to $L = 14$ rungs. DMRG is car-
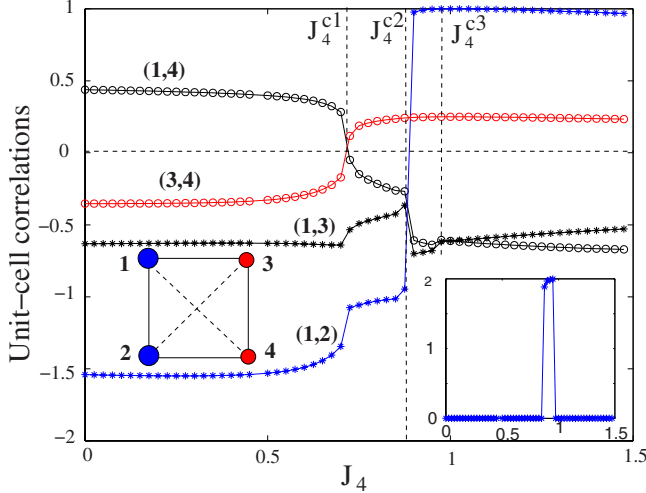
FIG. 3. (Color online) Unit-cell isotropic spin-spin correlations as a function of the frustration parameter J_4, as obtained from the DMRG method for open boundary conditions ($L=100$). $J_4^{c1}=0.710$, $J_4^{c2}=0.875$, and $J_4^{c3}=0.975$ are the special points identified as phase-transition points between different ground states. The inset shows the difference in the spin-1 rung correlations in two neighboring cells. Note that the presented spin-spin correlations belong to unit cells far from the ends.

ried out for this system for a range of lattice sizes up to $L=100$ rungs with the spin values $S_1=1$ and $S_2=1/2$, respectively. Up to 320 density-matrix eigenvectors were retained. Depending on the value of J_4, the truncation errors are between 10^{-7} and 10^{-12}.

The DMRG results presented in Fig. 3 reveal three special points on the J_4 axis separating regions with different characteristics of the short-range correlations: $J_4^{c1}=0.710$, $J_4^{c2}=0.875$, and $J_4^{c3}=0.975$. The same points are also presented in Fig. 4 which shows DMRG results ($L=90$) for the ground-state energy of the mixed-spin model (1). A detailed numeri-
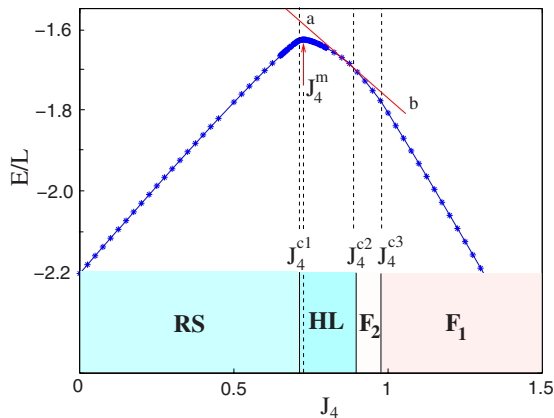
FIG. 4. (Color online) Ground-state energy per rung as a function of the frustration parameter J_4 (DMRG, $L=90$). $J_4^m=0.723$ denotes the location of the maximum. The positions of the special points identified in Fig. 3 separate different ground states: RS (rung-singlet), HL (Haldane-type), and two different ferrimagnetic states (F_1 and F_2). The straight line ab represents the energy of the Haldane state ($|\Psi_H\rangle$) defined by $E_H=\langle\Psi_H|\mathcal{H}|\Psi_H\rangle$.

cal analysis, using both the DMRG and ED methods, predicts singlet ground states in the entire region $0 \leq J_4 < J_4^{c2}$. For $J_4 > J_4^{c2}$, the same analysis suggests ground states characterized by net ferromagnetic moments. Below we argue that these special points are related to quantum phase transitions between different ground states.

A. Mapping onto the frustrated spin-$\frac{1}{2}$ ladder

An inspection of the short-range correlations presented in Fig. 3 implies that the weight of the local rung quintet (i.e., $s_{2n}=2$) states on the spin-1 rungs is negligible almost in the whole interval $0 \leq J_4 < J_4^{c2}$. Indeed, by using the identity $\langle s_{1,2n} \cdot s_{2,2n}\rangle=(\langle s_{2n}^2\rangle-3/2)/2-5/4$, one finds that the following relation between the average rung correlations should be satisfied for any state with a zero weight of the rung quintet states,

$$\langle s_{1,2n} \cdot s_{2,2n}\rangle = \langle \sigma_{1,2n-1} \cdot \sigma_{2,2n-1}\rangle - \frac{5}{4}. \quad (8)$$

As seen from the numerical results, the above relation is almost perfectly fulfilled in the entire region $0 \leq J_4 < J_4^{c2}$, excluding some narrow vicinity of the point J_4^{c2} where the correlations $\langle s_{1,2n} \cdot s_{2,2n}\rangle$ abruptly change to ≈ 1. The extremely small contribution of the quintet rung states in the region $0 \leq J_4 < J_4^{c2}$ can be explained by the peculiarities of the energy spectrum of the mixed-spin plaquette, where the lowest quintet state happens to be well separated from the low-lying triplet and singlet states. Note that the excitation of local quintet states is controlled by the last term (V) in Hamiltonian (2). Thus, starting from an eigenstate belonging to the sector $s_{2n}, \sigma_{2n-1}=0, 1$ ($n=1,\ldots,L/2$), the first-order corrections to the wave function of this eigenstate will contain relatively small amount of configurations belonging to the sectors with local quintet states due to the larger energy denominator in the perturbation expression.

These observations suggest, in particular, that in the discussed region the ground-state properties of the mixed-spin system may be approximately interpreted by projecting out the local quintet states in the mixed-spin Hamiltonian (2). Up to first order in J_a, the projected Hamiltonian reads as (see the Appendix)

$$\mathcal{H}_{eff}=-\frac{5}{8}JL + \sum_{n=1}^{L}[J'_\perp \sigma_{1,n} \cdot \sigma_{2,n} + J'_s \sigma_n \cdot \sigma_{n+1} + J'_a l_n \cdot l_{n+1}],$$

$$(9)$$

where $\sigma_{1,n}$ and $\sigma_{2,n}$ are spin-$\frac{1}{2}$ operators, $\underline{\sigma_n=\sigma_{1,n}+\sigma_{2,n}}$, $l_n=\sigma_{1,n}-\sigma_{2,n}$, $J'_\perp=J_\perp$, $J'_s=J_s$, and $J'_a=-2\sqrt{2/3}J_a$. For simplicity, we have restricted ourselves to the case of equal rung couplings ($J_1=J_2\equiv J_\perp$). The effective Hamiltonian (9) describes a frustrated spin-$\frac{1}{2}$ Heisenberg ladder characterized by three parameters, i.e., the strength of the rung ($J'_\perp$), leg ($J'_3=J'_s+J'_a$), and diagonal ($J'_4=J'_s-J'_a$) exchange bonds. Using the same reasoning, it may be safely suggested that the next-order corrections in J_a do not change substantially the singlet ground states, so that the effective Hamiltonian (9) may be used (i) to identify the singlet ground states of the
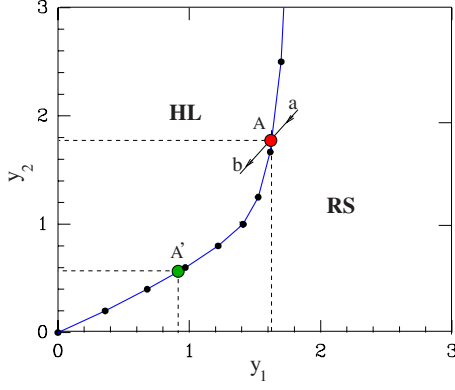
FIG. 5. (Color online) Phase diagram of the effective spin-$\frac{1}{2}$ ladder model with diagonal bonds (Ref. [30]). The point A with coordinates $(y_1, y_2) = (1.618, 1.766)$ is the image of the special point $J_4^{c1} = 0.710$ obtained by using Eq. (10). The point A' is an image of A corresponding to the symmetry transformation $J_3' \leftrightarrow J_4'$. ab is the path in the (y_1, y_2) plane corresponding to the change in J_4 at fixed $J_\perp = J_3 = 1$.

original Hamiltonian (2) in the region $0 \leq J_4 < J_4^{c2}$ and (ii) to analyze the related quantum phase transitions.

As is well known, as a function of the frustration parameter J_4' model (9) exhibits the so-called RS and Haldane-type (HL) phases.[4,30,33–37] Both ground states are nondegenerate and exhibit finite singlet-triplet gaps. The character of the quantum RS-HL transition in the weak-coupling limit is still under debate: some of the cited works[30,33,35,36] suggest a direct first-order transition between these phases but the others predict an intermediate columnar dimer phase.[4,34,37] Thus the mapping of Eq. (2) implies that the special point $J_4 = J_4^{c1}$ can presumably be identified as a quantum phase-transition point separating similar phases. Of course, such an analysis does not exclude the presence of some intermediate singlet phases in a tiny interval between the RS and HL states. Some hints in this direction inspired by the DMRG results for the ground-state energy (Fig. 4) will be discussed below in more detail.

The established connection with the frustrated spin-$\frac{1}{2}$ ladder model is additionally supported by the fact that the special point J_4^{c1} perfectly maps on the RS-HL phase boundary in the phase diagram of the frustrated spin-$\frac{1}{2}$ ladder model.[30] Indeed, taking the parameters $y_1 = J_\perp' / J_3'$ and $y_2 = J_4' / J_3'$ used in Ref. [30], the established relations $J_s' = J_s$ and $J_a' = -2\sqrt{2/3} J_a$ between the parameters of the original and the projected Hamiltonians take the form

$$y_1 = \frac{J_\perp / J_3}{b_2 J_4 / J_3 - b_1}, \quad y_2 = \frac{b_2 - b_1 J_4 / J_3}{b_2 J_4 / J_3 - b_1}, \quad (10)$$

where $b_1 = \sqrt{2/3} - 1/2$ and $b_2 = \sqrt{2/3} + 1/2$. Note that the change in J_4 (at fixed $J_\perp = J_3 = 1$) corresponds to a run in the (y_1, y_2) plane on the ab line (see Fig. 5) defined by $y_2 = (b_1/b_2 + 1)y_1 - b_1/b_2$. Following Ref. [30], we may identify the position of the quantum phase transition with the point $J_4 = J_4^{c1} \equiv 0.710$ where the spin-$\frac{1}{2}$ rung correlations change their sign (see Fig. 3). We find that the (y_1, y_2) image A of the transition point J_4^{c1} maps perfectly on the phase boundary in
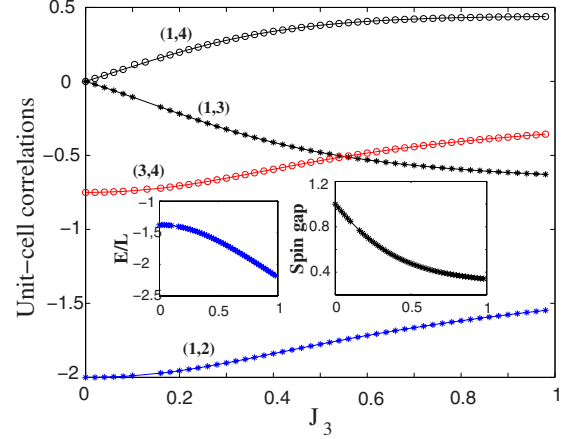
FIG. 6. (Color online) Unit-cell isotropic spin-spin correlations of model (1) as a function of $J_3(J_4 = 0, L = 100)$. The notations are defined in Fig. 3. The inset on the left shows the ground-state energy per rung vs J_3 and the inset on the right shows the variation in the singlet-triplet excitation gap with J_3.

the (y_1, y_2) plane. In Fig. 5, we also show the symmetric point A' obtained by the coordinate transformations $y_1 \rightarrow y_1/y_2$ and $y_2 \rightarrow 1/y_2$, which are related to the exchange symmetry $J_3 \leftrightarrow J_4$ of the Hamiltonian. As expected, the symmetric point A' also lies on the phase boundary.

B. Rung-singlet and Haldane-type phases

1. Rung-singlet phase

The RS phase, originally studied in the two-leg spin-$\frac{1}{2}$ ladder without diagonal bonds,[38,39] is a nondegenerate singlet state with a finite singlet-triplet gap. The existence of a spin gap in this model can be easily anticipated by using a strong-coupling analysis:[39] for $J_3'/J_\perp' \ll 1$, the ground state is a simple product of rung singlet bonds. The lowest rung excited states are local triplets with a characteristic gap $\propto J_\perp'$ which survives the perturbation in $J_3'/J_\perp'$. On the other hand, the perturbation produces an energy band (with a bandwidth $\propto J_3'$) of triplet excitations.

The same physics can be easily extracted from a strong-coupling analysis of the mixed-spin ladder, Eq. (2). Instead of doing this, we present in Fig. 6 DMRG results for the short-range correlations as a function of $J_3(J_4 = 0)$. The state at $(J_3, J_4) = (1, 0)$ is known to be gapped.[40] The essential information in Fig. 6 is that the curves are devoid of any features that might suggest a change in the phase. Thus we can assert that the phase at $J_3 = 1$ is smoothly connected to the phase at $J_3 = 0$, which is a RS phase. The variation in the gap with J_4 is shown in Fig. 7. We see that the gap goes to zero around the point $J_4 = 0.710$ identified above as a phase transition point to another singlet phase. Below we discuss in more detail the structure of the low-lying excitations close to $J_4 = J_4^{c1}$.

2. Haldane-type phase

The discussed mapping of Eq. (2) on the frustrated spin-$\frac{1}{2}$ ladder model suggests that the HL phase should occupy some
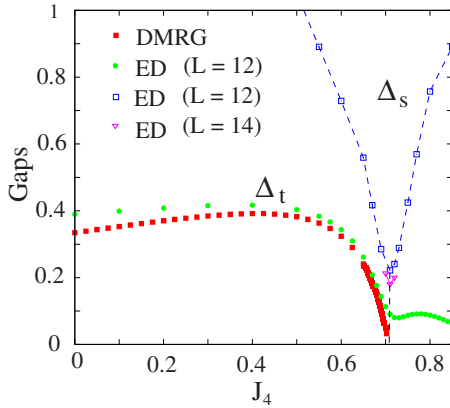
FIG. 7. (Color online) DMRG and ED numerical results for the singlet-singlet (Δ_s) and singlet-triplet (Δ_s) excitation gaps in the mixed-spin model (1) vs J_4. The DMRG data points correspond to extrapolated values of Δ_s obtained by a polynomial fit (up to L =90) for open boundary conditions. The ED data concerns periodic clusters with L=10, 12, and 14.

region in the phase diagram for $J_4 > J_4^{c1}$. To reveal the peculiarities of the suggested HL phase—as compared to the well-known Haldane phase of the periodic spin-1 Heisenberg chain—notice that in the sector $[1,1,\ldots,1]$ the Haldane state $|\Psi_H\rangle$ is the exact ground state of the mixed-spin Hamiltonian (2) at the symmetric point $J_3 = J_4$. In the general case ($J_3 \neq J_4$), the energy of this state $E_H = \langle \Psi_H | \mathcal{H} | \Psi_H \rangle$ reads as

$$\frac{E_H}{L} = -\frac{J_1}{2} + \frac{J_2}{8} + \frac{1}{2}(J_3 + J_4)\varepsilon_H, \quad (11)$$

where $\varepsilon_H = -1.40148403897(4)$ is the ground-state energy per bond of the periodic spin-1 Heisenberg chain.[41] Here, we have used the fact that the operator V [Eq. (3)] does not have nonzero matrix elements in the sector $[1,1,\ldots,1]$: in particular, we have $\langle \Psi_H | V | \Psi_H \rangle = 0$. The energy of the Haldane state E_H as a function of J_4 ($J_1 = J_2 = J_3 = 1$) is shown in Fig. 4 (the ab line). Interestingly, at the special point $J_4 = J_4^{c2} \equiv 0.875$—also related to an abrupt change in the spin-1 rung correlations—the DMRG estimate for the ground-state energy of Hamiltonian (2) $E/L = -1.6899$ almost coincides with the energy of the Haldane state ($E_H/L = -1.6889$) obtained from Eq. (11). As already mentioned above, the numerical analysis implies that the special point J_4^{c2} is a quantum phase-transition point from a singlet nondegenerate state to a state exhibiting a net magnetic moment. The above remarks suggest that the HL phase appears as a good candidate for the phase diagram of the mixed-spin model.

Further qualitative information about the characteristics of this phase can be extracted from a perturbative analysis starting from the symmetric point $J_3 = J_4$ and based on the Haldane state in a periodic spin-1 chain. Note that in some interval ($J_4 < J_4^{c2}$) the parameter J_a, which controls the V term in Eq. (2), may be used as a small parameter (e.g., J_a =0.0625 for J_4=0.875). Thus, up to second order in J_a, the ground-state energy takes the form $E = E_H - \text{const}(1 - J_4)^2 L$, where const is some positive number of order 1. Qualitatively, this result reproduces the behavior of the ground-state

energy in the interval $J_4^{c1} < J_4 < J_4^{c2}$ extracted from the DMRG analysis (see Fig. 4). To some extent, this result also validates the choice of $|\Psi_H\rangle$ as a starting unperturbed state.

As compared to the Haldane state, some peculiarities of the HL phase can be revealed by looking at the first-order correction in J_a to the wave function $|\Psi_H\rangle$,

$$|\Psi\rangle = |\Psi_H\rangle + J_a \sum_{n \neq 0} \frac{\langle \Psi_n | V | \Psi_H \rangle}{E_0 - E_n} |\Psi_n\rangle + \mathcal{O}(J_a^2). \quad (12)$$

Here the sum runs over the excited eigenstates $|\Psi_n\rangle$ of Hamiltonian (2) at $J_3 = J_4$, and $E_0 \equiv E_H$. The matrix elements of V (see the Appendix) admit only two types of excited states ($|\Psi_{1,2}\rangle$) defined, respectively, in the sectors $[1,\ldots 1,0,0,1,\ldots,1]$ (two neighboring rungs in singlet states) and $[1,1,\ldots,1,2,0,1,\ldots,1]$ (one rung in a quintet state an a neighboring rung in a singlet state). The weights of both types of defect configurations in the HL state change in the interval $J_4^{c1} < J_4 < J_4^{c2}$: while the weight of the $|\Psi_1\rangle$ configurations grows in a region around the transition point J_4^{c1}, the $|\Psi_2\rangle$ configurations (containing spin-2 defects) become visible in the DMRG result for the spin-1 rung correlations only in a short interval preceding the transition to a magnetic state (see Fig. 3). Note that the observed increase in the weight of the $|\Psi_2\rangle$ configurations formally contradicts the perturbation result in Eq. (12), which predicts the opposite behavior. A reasonable resolution for this is provided by the guess that close to the transition point J_4^{c2} some of the eigenenergies E_n related to the sector $[1,1,\ldots,1,2,0,1\ldots,1]$ soften. As of now we do not have firm numerical results in favor of such a suggestion, although some preliminary DMRG results, using open boundary conditions, seem to predict strong reductions in the singlet-quintet and triplet-quintet gaps close to J_4^{c2}.

3. RS-HL transition

Turning to the region around the transition point J_4^{c1}, it is instructive to comment on our numerical results for the excitation gaps (Fig. 7) in the light of the discussed mapping to the spin-$\frac{1}{2}$ ladder model. For the latter model, it has been numerically established[30] that (i) the lowest state above the singlet ground states close to the phase boundary is a singlet excitation and (ii) the low-lying triplet excitations are gapped in the whole region of the phase diagram in Fig. 5, including the phase-transition boundary. Such a structure of the low-lying excitations is consistent with the established first-order quantum phase transition, which is described as a level crossing of two singlet ground states. As already mentioned, the character of the RS-HL transition in the weak-coupling limit ($J'_{\perp}, J'_4 \ll J'_3$) is still under debate.[4,36,37] As a matter of fact, there are some indications for a second-order RS-HL transition[4] and an intermediate dimer phase,[34,37] but the debate concerns only the weak-coupling part of the phase boundary. Looking at the coordinates of the A and A' images of the transition point J_4^{c1} (Fig. 5), it is clearly seen that the discussed RS-HL transition at $J_4 = J_4^{c1}$ does not belong to the weak-coupling region. Hence, one may expect a first-order RS-HL transition at J_4^{c1} related to a level crossing of singlet ground states.
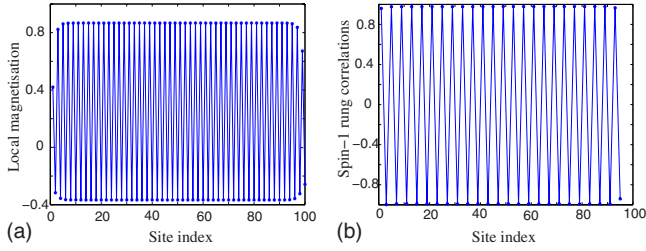
FIG. 8. (Color online) (a) The local magnetizations $\langle s_{1,2n}^z \rangle$ and $\langle \sigma_{1,2n+1}^z \rangle (n=1,\ldots,50)$ along the first leg as a function of the site index. The data shown is for $J_4=1.55$. (b) The spin-1 rung correlations along the length of the ladder ($L=100$) at $J_4=0.90$. The values show a clear alternation between ≈ 1 and ≈ -1 which indicates a two sublattice structure and a doubled unit cell containing four rungs.

Figure 7 presents our numerical (DMRG and ED) results for the singlet (Δ_s) and triplet (Δ_t) gaps of the lowest excited modes above both singlet ground states. Let us first discuss the ED data for the gaps. As clearly seen, both minima, related to the Δ_s and Δ_t data points, are located close to the expected transition point at $J_4=0.710$. More importantly, an extrapolation of the ED data for $J_4=0.710$ implies that the Δ_s points scale to smaller values than Δ_t. This observation is consistent with the expected low-energy structure close the first-order transition point between the RS and HL phases.

Turning to the DMRG results for $\Delta_t(J_4)$, one observes that the triplet gap of the RS phase takes very small values close to the suggested transition point ($J_4=0.710$). We could not conclusively exclude the possibility of a gapless triplet excitation at the transition point. In any case, such a behavior indicates some peculiarities of the RS-HL transition in the mixed-spin system, as compared to the uniform-spin case. Another issue to be noticed is the steep (but definitely finite) slope of the function $\Delta_t(J_4)$ at the transition point. This suggests a relatively large correlation length of this triplet excitation close to J_4^{c1}.

C. Ferrimagnetic phases

Looking at the DMRG results for the short-range correlations (Fig. 3), it is easy to realize that a ferrimagnetic phase, closely related to the ferrimagnetic ground state of an antiferromagnetic Heisenberg chain with alternating $(2,1)$ spins, is stabilized around the symmetric point $J_4=1$. Exactly at $J_4=1$, the ground state of Hamiltonian (2) belongs to the sector $[1,2,\ldots,1,2]$, so that both models are equivalent in the low-energy sector of the spectrum. The discussed ferrimagnetic phase (F_1) exhibits the magnetic moment per rung $M_0=1/2$ and survives almost in the entire region after J_4^{c2}, excluding some narrow interval in the vicinity of the latter point. This is also seen in Fig. 8(a) which shows a typical behavior of the local magnetizations $\langle s_{1,2n}^z \rangle$ and $\langle \sigma_{1,2n+1}^z \rangle$ ($n=1,\ldots,L/2$) along the first leg at $J_4=1.55$. The values of the spin-1 and spin-$\frac{1}{2}$ magnetic moments are 0.866950 and -0.366950, respectively. We see that the sum of the local magnetic moments is $1/2$, as expected in a Lieb-Mattis-type ferrimagnetic state with a quantized magnetic moment per

rung $M_0=1/2$. The deviations at the end are essentially because of open boundary conditions. We have verified numerically that these values do not change much after $J_4=1$.

For the region close to J_4^{c2}, the DMRG results presented in Fig. 8(b) demonstrate the appearance of another ferrimagnetic phase (F_2) in a narrow range of J_4 starting from the transition point $J_4^{c2}=0.875$ and terminating at $J_4^{c3}=0.975$. The F_2 phase is characterized by the magnetic moment per rung $M_0=1/4$. As clearly seen in Fig. 8(b), in the F_2 phase the space variation in the spin-1 rung correlations follow strictly the periodicity of the spin structure in the sector $[2,1,1,1,\ldots,2,1,1,1]$. Such a breaking of the translational symmetry is also seen in the inset of Fig. 3, where on the vertical axis we have plotted the magnitude of the difference of the spin-1 rung correlations in two neighboring unit cells for all values of J_4. Clearly, the F_2 phase represents a two-fold degenerate ground state, which is invariant under the translation by two lattice periods. Our numerical analysis does not support the appearance of ferrimagnetic phases with larger periods.

IV. CONCLUSION

In conclusion, we have analyzed the combined effect of the quantum fluctuations and the competing interactions in a mixed-spin ladder composed of spin-1 and spin-$\frac{1}{2}$ rungs which is closely related to a recently synthesized quasi-1D ferrimagnetic material. A comparison of the classical and quantum phase diagrams reveals the following changes in the related quantum system. As expected, the classical ferrimagnetic phase is also present in the quantum phase diagram but there appears another twofold degenerate ferrimagnetic state which breaks the translational symmetry. As may be expected, the classical Néel state does not survive quantum fluctuations. More interestingly, the classical canted state also completely disappears. This is in contrast to some other 1D spin systems exhibiting classical canted states,[6] where this type of classical magnetic order partially survives quantum fluctuations. In the present case, both the classical long-range ordered states are replaced by two singlet nondegenerate gapped states (RS and HL).

Turning to the weakly frustrated region, it has been established that the behavior of the system strongly resembles that of a two-leg spin-$\frac{1}{2}$ Heisenberg ladder with frustrating diagonal interactions. However, concerning the quantum phase transition between the RS and HL phases, we have found a few indications demonstrating some peculiarities (such as the extremely small triplet gap at the transition point) of the mixed-spin system. These issues deserve further investigations.

Finally, although the available experimental results on the ferrimagnetic ladder material $Fe^{II}Fe^{III}$ (trans-1,4-cyclohexanedicarboxylate) seem to point toward the realization of the F_1 ferrimagnetic state,[15] a detailed comparison with the experiment requires a more extensive analysis of the quantum phase diagram including, e.g., different rung couplings $J_1 \neq J_2$, different pairs of rung spin magnitudes, and some anisotropies. Concerning the condition $J_3=1$, as shown in Fig. 5 it simply restricts the path in the more general

parameter space ($J_3 \neq 1$) to a straight line crossing one and the same phase boundary. Therefore, there should be a relatively large region with $J_3 \neq 1$ showing the same structure of the phase diagram. As to the second restriction ($J_1 = J_2$), its removal may be generally expected to bring new quantum spin phases. However, in both cases we have numerically checked that relatively small deviations from the conditions $J_1 = J_2 = J_3$ do not bring qualitative changes on the established quantum phase diagram.

APPENDIX: PROJECTION ONTO THE SPIN-$\frac{1}{2}$ LADDER

We have to project the spin-1 rung states onto the states of the spin-$\frac{1}{2}$ rungs. To this end, we use the projection operator $P = P_1 P_2, \ldots, P_L$, where the rung projection operator P_n reads as

$$P_n = \sum_\alpha |T_{2n}^\alpha\rangle\langle T_{2n}^\alpha|, \quad \alpha = 0, x, y, z. \tag{A1}$$

Here $|T_{2n}^0\rangle$ denotes the singlet state of the $2n$th spin-1 rung and $|T_{2n}^k\rangle = (i/\sqrt{2})\epsilon^{klm}|l\rangle|m\rangle$ are the triplet states of the same rung in a vector basis which is a tensor product of the vector bases of the spin-1 objects (i.e., $|x\rangle$, $|y\rangle$, and $|z\rangle$). In the following, the Greek indices take the values 0, x, y, and z, whereas the Latin ones—x, y, and z.

Up to first order in J_a, the projected Hamiltonian reads as

$$\mathcal{H}_{eff} = P\mathcal{H}P. \tag{A2}$$

By using the expressions for the matrix elements $\langle T_{2n}^m|s_{2n}^2|T_{2n}^n\rangle = 2\delta^{mn}$, $\langle T_{2n}^0|L_{2n}^k|T_{2n}^0\rangle = \langle T_{2n}^m|L_{2n}^k|T_{2n}^l\rangle = 0$, and $\langle T_{2n}^m|L_{2n}^k|T_{2n}^0\rangle = -2\sqrt{2/3}\delta^{mk}$, one obtains

$$P_n s_{2n}^2 P_n = 2\sum_k |T_{2n}^k\rangle\langle T_{2n}^k| = \sigma_{2n}^2, \tag{A3}$$

where σ_{2n} is an effective rung-$\frac{1}{2}$ spin operator, and

$$P_n V_n P_n = -2\sqrt{\frac{2}{3}}\sum_k [|T_{2n}^0\rangle\langle T_{2n}^k| + |T_{2n}^k\rangle\langle T_{2n}^0|](l_{2n-1}^k + l_{2n+1}^k).$$

Note that the operator in the square brackets is an effective l_{2n} rung vector operator for spin-$\frac{1}{2}$ rungs. Summing the above results, we obtain the effective spin-$\frac{1}{2}$ ladder model presented in Eq. (9).

[1] *Frustrated Spin Systems*, edited by H. T. Diep (World Scientific, Singapore, 2004).

[2] *Quantum Magnetism*, Lecture Notes in Physics Vol. 645, edited by U. Schollwöck, J. Richter, D. J. J. Farnell, and R. F. Bishop (Springer, Berlin, 2004).

[3] S. R. White, Phys. Rev. B **53**, 52 (1996); E. H. Kim, G. Fáth, J. Sólyom, and D. J. Scalapino, *ibid.* **62**, 14965 (2000); G. Fáth, O. Legeza, and J. Sólyom, *ibid.* **63**, 134403 (2001).

[4] O. A. Starykh and L. Balents, Phys. Rev. Lett. **93**, 127202 (2004).

[5] D. Allen, F. H. L. Essler, and A. A. Nersesyan, Phys. Rev. B **61**, 8871 (2000).

[6] N. B. Ivanov, Condens. Matter Phys. **12**, 435 (2009).

[7] K. Sengupta and Y. B. Kim, Phys. Rev. B **71**, 174427 (2005).

[8] O. Kahn, *Molecular Magnetism* (Wiley-VCH, New York, 1993).

[9] S. K. Pati, S. Ramasesha, and D. Sen, Phys. Rev. B **55**, 8894 (1997); J. Phys.: Condens. Matter **9**, 8707 (1997).

[10] S. Brehmer, J.-H. Mikeska, and S. Yamamoto, J. Phys.: Condens. Matter **9**, 3921 (1997); A. K. Kolezhuk, H.-J. Mikeska, and S. Yamamoto, Phys. Rev. B **55**, R3336 (1997).

[11] N. B. Ivanov, Phys. Rev. B **57**, R14024 (1998).

[12] M. Hagiwara, K. Minami, Y. Narumi, K. Tatani, and K. Kindo, J. Phys. Soc. Jpn. **67**, 2209 (1998).

[13] H. Nishide, Adv. Mater. (Weinheim, Ger.) **7**, 937 (1995).

[14] J. B. Anderson, E. Kostiner, and F. A. Ruszala, J. Solid State Chem. **39**, 29 (1981); A. Boukhari, A. Moqine, and S. Flandrois, Mater. Res. Bull. **21**, 395 (1986); H. Effenberger, J. Solid State Chem. **142**, 6 (1999); S. Yamamoto and J. Ohara, Phys. Rev. B **76**, 014409 (2007).

[15] Y.-Z. Zheng, W. Xue, W.-X. Zhang, M.-L. Tong, X.-M. Chen, F. Grandjean, G. J. Long, S.-W. Ng, P. Panissod, and M. Drillon, Inorg. Chem. **48**, 2028 (2009).

[16] K. Takano, K. Kubo, and H. Sakamoto, J. Phys.: Condens. Matter **8**, 6405 (1996); H. Niggemann, G. Uimin, and J. Zittartz, *ibid.* **9**, 9031 (1997).

[17] K. Okamoto, T. Tonegawa, Y. Takahashi, and M. Kaburagi, J. Phys.: Condens. Matter **11**, 10485 (1999); K. Okamoto, T. Tonegawa, and M. Kaburagi, *ibid.* **15**, 5979 (2003); H.-J. Mikeska and C. Luckmann, Phys. Rev. B **77**, 054405 (2008).

[18] H. Ohta, S. Okubo, T. Kamikawa, T. Kunimoto, Y. Inagaki, H. Kikuchi, T. Saito, M. Azuma, and M. Takano, J. Phys. Soc. Jpn. **72**, 2464 (2003); H. Kikuchi, Y. Fujii, M. Chiba, S. Mitsudo, T. Idehara, T. Tonegawa, K. Okamoto, T. Sakai, T. Kuwai, and H. Ohta, Phys. Rev. Lett. **94**, 227201 (2005).

[19] T. Tonegawa, K. Okamoto, T. Hikihara, Y. Takahashi, and M. Kaburagi, J. Phys. Soc. Jpn. **69**, Suppl. A, 332 (2000).

[20] N. B. Ivanov, J. Richter, and J. Schulenburg, Phys. Rev. B **79**, 104412 (2009).

[21] N. B. Ivanov, J. Richter, and U. Schollwöck, Phys. Rev. B **58**, 14456 (1998); T. Kuramoto, J. Phys. Soc. Jpn. **73**, 2518 (2004).

[22] A. V. Chubukov, Phys. Rev. B **44**, 4693 (1991); F. Heidrich-Meisner, A. Honecker, and T. Vekua, *ibid.* **74**, 020403(R) (2006); D. V. Dmitriev, V. Ya. Krivnov, and J. Richter, *ibid.* **75**, 014424 (2007); D. V. Dmitriev and V. Ya. Krivnov, *ibid.* **77**,

024401 (2008); M. Härtel, J. Richter, D. Ihle, and S.-L. Drechsler, *ibid.* **78**, 174412 (2008); J. Sudan, A. Luscher, and A. M. Läuchli, *ibid.* **80**, 140402(R) (2009).

23 M. Hase, H. Kuroe, K. Ozawa, O. Suzuki, H. Kitazawa, G. Kido, and T. Sekine, Phys. Rev. B **70**, 104426 (2004).

24 S.-L. Drechsler, O. Volkova, A. N. Vasiliev, N. Tristan, J. Richter, M. Schmitt, H. Rosner, J. Málek, R. Klingeler, A. A. Zvyagin, and B. Büchner, Phys. Rev. Lett. **98**, 077202 (2007).

25 M. Enderle, C. Mukherjee, B. Fak, R. K. Kremer, J.-M. Broto, H. Rosner, S.-L. Drechsler, J. Richter, J. Malek, A. Prokofiev, W. Assmus, S. Pujol, J.-L. Raggazoni, H. Rakato, M. Rheinstädter, and H. M. Ronnow, Europhys. Lett. **70**, 237 (2005).

26 Y. Naito, K. Sato, Y. Yasui, Y. Kobayashi, Y. Kobayashi, and M. Sato, J. Phys. Soc. Jpn. **76**, 023708 (2007).

27 M. G. Banks, F. Heidrich-Meisner, A. Honecker, H. Rakoto, J.-M. Broto, and R. K. Kremer, J. Phys.: Condens. Matter **19**, 145227 (2007).

28 A. Langari and M. A. Martín-Delgado, Phys. Rev. B **63**, 054432 (2001); N. B. Ivanov and J. Richter, *ibid.* **69**, 214420 (2004); **73**, 132407 (2006).

29 V. R. Chandra, D. Sen, N. B. Ivanov, and J. Richter, Phys. Rev. B **69**, 214406 (2004); S. Yoshikawa and S. Miyashita, J. Phys. Soc. Jpn. **74**, 71 (2005); K. Hida, *ibid.* **76**, 024714 (2007); J. Phys.: Condens. Matter **19**, 145225 (2007); K. Hida and K.

Takano, Phys. Rev. B **78**, 064407 (2008); R. R. Montenegro-Filho and M. D. Coutinho-Filho, *ibid.* **78**, 014418 (2008).

30 Z. Weihong, V. Kotov, and J. Oitmaa, Phys. Rev. B **57**, 11439 (1998).

31 M. P. Gelfand, Phys. Rev. B **43**, 8644 (1991); A. Honecker, F. Mila, and M. Troyer, Eur. Phys. J. B **15**, 227 (2000); V. R. Chandra and N. Surendran, Phys. Rev. B **74**, 024421 (2006).

32 S. R. White, Phys. Rev. Lett. **69**, 2863 (1992); Phys. Rev. B **48**, 10345 (1993).

33 X. Wang, Mod. Phys. Lett. B **14**, 327 (2000).

34 T. Vekua and A. Honecker, Phys. Rev. B **73**, 214427 (2006).

35 H.-H. Hung, C.-D. Gong, Y.-C. Chen, and M.-F. Yang, Phys. Rev. B **73**, 224433 (2006).

36 E. H. Kim, O. Legeza, and J. Sólyom, Phys. Rev. B **77**, 205121 (2008).

37 G.-H. Liu, H.-L. Wang, and G.-S. Tian, Phys. Rev. B **77**, 214418 (2008).

38 E. Dagotto, J. Riera, and D. J. Scalapino, Phys. Rev. B **45**, 5744 (1992).

39 T. Barnes, E. Dagotto, J. Riera, and E. S. Swanson, Phys. Rev. B **47**, 3196 (1993).

40 A. E. Trumper and C. Gazza, Phys. Rev. B **64**, 134408 (2001).

41 S. R. White and D. A. Huse, Phys. Rev. B **48**, 3844 (1993).